An Engineered Transthyretin Monomer that Is Nonamyloidogenic, Unless It Is Partially Denatured†

Xin Jiang,‡ Craig S. Smith,§ H. Michael Petrassi,‡ Per Hammarström,‡ Joleen T. White,‡ James C. Sacchettini,§ and Jeffery W. Kelly*,‡

Department of Chemistry and The Skaggs Institute of Chemical Biology, The Scripps Research Institute, La Jolla, California 92037, and Department of Biochemistry and Biophysics, Texas A&M University, College Station, Texas 77843

Received June 8, 2001; Revised Manuscript Received July 25, 2001

ABSTRACT: Transthyretin (TTR) is a soluble human plasma protein that can be converted into amyloid by acid-mediated dissociation of the homotetramer into monomers. The pH required for disassembly also results in tertiary structural changes within the monomeric subunits. To understand whether these tertiary structural changes are required for amyloidogenicity, we created the Phe87Met/Leu110Met TTR variant (M-TTR) that is monomeric according to analytical ultracentrifugation and gel filtration analyses and nonamyloidogenic at neutral pH. Results from far- and near-UV circular dichroism spectroscopy, one-dimensional proton NMR spectroscopy, and X-ray crystallography, as well as the ability of M-TTR to form a complex with retinol binding protein, indicate that M-TTR forms a tertiary structure at pH 7 that is very similar if not identical to that found within the tetramer. Reducing the pH results in tertiary structural changes within the M-TTR monomer, rendering it amyloidogenic, demonstrating the requirement for partial denaturation. M-TTR exhibits stability toward acid and urea denaturation that is nearly identical to that characterizing wild-type (WT) TTR at low concentrations (0.01−0.1 mg/mL), where monomeric WT TTR is significantly populated at intermediate urea concentrations prior to the tertiary structural transition. However, the kinetics of denaturation and fibril formation are much faster for M-TTR than for tetrameric WT TTR, particularly at near-physiological concentrations, because of the barrier associated with the tetramer to folded monomer preequilibrium. These results demonstrate that the tetramer to folded monomer transition is insufficient for fibril formation; further tertiary structural changes within the monomer are required.

Amyloid diseases are putatively caused by the aberrant self-assembly of one of twenty human proteins or a fragment(s) thereof into amyloid fibrils (*1*−*6*). The twenty human amyloidogenic proteins share no apparent sequence, structural, or functional homology, yet they all form a similar cross-β-sheet quaternary structure (*7*, *8*). In cases where normally folded full-length proteins compose the fibrils (e.g., transthyretin, lysozyme variants, immunoglobulin light chain, and β_2-microglobulin), a denaturing stress and/or a mutation leads to a conformational change affording an intermediate that self-assembles into amyloid (*1*, *2*, *5*, *9*, *10*). The amyloidogenic conformational intermediates that have been characterized to date either are rich in β-sheet structure or have the capacity to become rich in β-sheet structure before (*11*) or upon oligomerization (*12*, *13*). Recent studies reveal that several nonamyloidogenic proteins can also form amyloid fibrils when placed under a sufficiently severe denaturing stress (*14*−*18*), implying that these proteins are capable of adopting conformations that are fibrilogenic.

Transthyretin (TTR)[1] is a homotetramer composed of 127 amino acid subunits characterized by 2,2,2 molecular symmetry. TTR is found in human plasma (0.1−0.4 mg/mL) and cerebral spinal fluid (0.017 mg/mL), the plasma form being the amyloidogenic precursor. Plasma TTR binds to the retinol binding protein (RBP)−vitamin A complex (typically ≤1 equiv/TTR tetramer), in addition to serving as a secondary carrier for the thyroid hormone thyroxine (5−10% of the TTR binding capacity). Crystallographic analysis reveals that each subunit has a β-sheet sandwich tertiary structure, one four-stranded β-sheet being stacked upon another four-stranded sheet. The subunits dimerize by intermolecular antiparallel β-sheet formation involving the H and H′ strands (Figure 1). Dimerization of these dimers is mediated by AB−GH loop interactions affording the tetramer. The AB−GH loop interface creates a channel through the tetramer wherein 2 molecules of thyroid hormone can bind.

† The authors gratefully acknowledge the National Institutes of Health (Grant DK46335), The Skaggs Institute of Chemical Biology, and the Lita Annenberg Hazen Foundation for the financial support of this work. P.H. thanks the Wenner-Gren Foundations for a post doctoral fellowship.

* To whom correspondence should be addressed: The Scripps Research Institute, BCC506, 10550 N. Torrey Pines Rd., La Jolla, CA 92037. E-mail: jkelly@scripps.edu. Fax: (858) 784-9610. Phone: (858) 784-9601.

‡ The Scripps Research Institute.

§ Texas A&M University.

[1] Abbreviations: TTR, transthyretin; WT, wild type; M-TTR, F87M/L110M TTR variant; ANS, 1-anilino-8-naphthalenesulfonate; DBF, 4,6-dibenzofurandicarboxylic acid; EM, electron microscopy; FAP, familial amyloid polyneuropathy; Flu, flufenamic acid; GdnHCl, guanidine hydrochloride; RBP−A, retinol binding protein−vitamin A complex; TFT, thioflavin T.

10.1021/bi011194d CCC: $20.00
Published on Web 08/24/2001

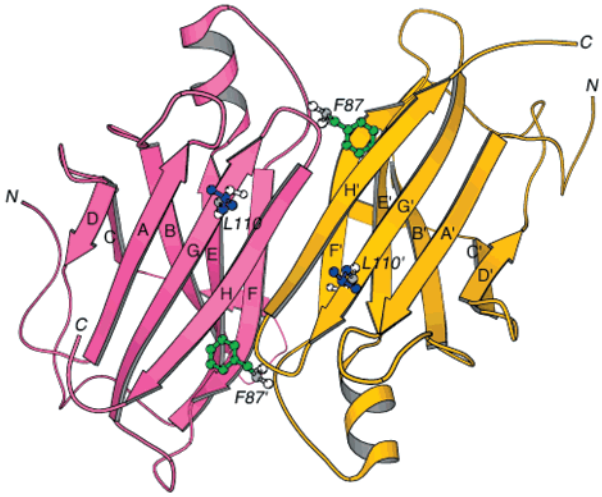

FIGURE 1: Ribbon diagram of the TTR dimer, looking down at the hydrophobic interface. The positions of the two residues (Phe87 and Leu110) that were mutated to Met to generate the monomeric variant are explicitly shown. The H strands from two adjacent monomers form the hydrogen-bonded interface resulting in the dimer shown here. Two dimers then interact through hydrophobic interactions to form a tetramer involving strands A, D, and G as well as the loop between strands G and H. This figure was generated using the program Molscript (*43*).

Wild-type (WT) TTR amyloidogenesis putatively causes senile systemic amyloidosis, characterized by deposition and pathology in the heart after age 60 (*19*). Early onset amyloid formation (as early as the second decade) by one of >80 single-site TTR variants appears to cause the diseases collectively termed familial amyloid polyneuropathy (FAP) (*20*), characterized by neuropathy and/or organ dysfunction. The FAP-associated variants characterized thus far (e.g., V30M and L55P TTR), although tetrameric, are destabilized (*21*). This destabilization allows tetramer dissociation to the amyloidogenic monomeric intermediate to occur under the influence of a mild denaturation stress (e.g., pH 5.2), where the WT TTR protein remains tetrameric and nonamyloidogenic. A comparison of the WT TTR crystal structure to more than 10 FAP variants reveals that the tertiary and quaternary structures are essentially identical (*22*), consistent with the partial denaturation requirement for amyloidogenesis. All of the FAP variants characterized to date adequately function as thyroid and retinol binding protein (RBP) transporters; hence, there is no evidence that FAP is a loss-of-function disease.

Even though a plethora of data support the hypothesis that it is the alternatively folded TTR monomer that is amyloidogenic, it has been difficult to eliminate the normally folded monomer, dimer, and tetramer as possible amyloid precursors because low concentrations of these species may exist under the acidic amyloid enabling conditions (*23*−*26*). Herein, we engineer a monomeric variant of TTR using a structure-based approach. A mutation is introduced into each of the two different types of subunit interfaces described above, which is envisioned to block tetramerization by steric clashing because of the conformational preferences of the Met side chain replacing the Phe87 and Leu110 side chains (M-TTR). Studies on the normally folded monomeric M-TTR variant reveal that it is not amyloidogenic at pH 7; however, partial acid denaturation enables rapid amyloid formation. These and other data make it clear that tertiary structural changes within the monomer are required for TTR amyloid formation.

MATERIALS AND METHODS

Protein Expression and Purification. The F87M and F87M/L110M (M-TTR) plasmids were prepared utilizing the QuickChange site-directed mutagenesis procedure from Stratagene (La Jolla, CA) using WT TTR DNA (Met^{-1}) as the template. Mutations were verified by DNA sequencing. Both the WT and mutant proteins were isolated and purified from recombinant sources following previously described procedures (*27*); all proteins were expressed as soluble forms in the cytoplasm. These TTR variants were further purified by gel filtration by employing a Superdex 75 gel filtration column (Amersham Pharmacia, Piscataway, NJ). The yield after purification of M-TTR is high, usually ∼10−30 mg/L of LB culture. Buffers composed of 50 mM sodium phosphate, 100 mM KCl, and 1 mM EDTA were employed for all the experiments unless otherwise mentioned. The concentrations of all protein solutions were determined by the absorbance at 280 nm, using an ϵ of 77 600 M^{-1} cm^{-1} for WT TTR and M-TTR.

Nuclear Magnetic Resonance. One-dimensional (1D) proton NMR spectra were collected on 5.5 mg/mL TTR samples in 50 mM sodium phosphate buffer (pH 6.3 and 25 °C) at 600 MHz. Water suppression was achieved with the watergate pulse sequence.

Analytical Ultracentrifugation. All sedimentation experiments were performed using a temperature-controlled Beckman XL-I analytical ultracentrifuge equipped with an An60Ti rotor and a photoelectric scanner. Typically, 0.4−2 mg/mL (28.8−144 $\mu M_{monomer}$) M-TTR solutions at pH 7 (50 mM phosphate, 100 mM KCl, and 1 mM EDTA) were used for both sedimentation equilibrium and velocity experiments. Sedimentation equilibrium measurements were taken using 120−140 μL volumes loaded into a double-sector cell equipped with a 12 mm Epon centerpiece and sapphire or quartz windows. Data were collected at a rotor speed of 27 000 rpm to allow equilibrium to be established across the cell. After equilibrium was reached, 20 scans were taken at a step size of 0.001 cm and averaged. Data analysis was carried out using a nonlinear least-squares analysis in the Origin software package provided by Beckman. For sedimentation velocity experiments, data were collected at speeds of 3000 and 50 000 rpm in the continuous mode at 20 °C, employing a step size of 0.001 cm. A direct boundary fitting approach was applied to evaluate the sedimentation velocity data. The DCDT+ program was used to fit multiple concentration versus radial position data sets simultaneously. The fitting algorithm yields the sedimentation coefficient and diffusion coefficient that affords the molecular mass using the following equation:

$$MW = SRT/D(1 - \bar{\nu}\rho) \quad (1)$$

where MW is the molecular mass (daltons), S is the sedimentation coefficient (in Svedbergs, 10^{-13} s), R is the universal gas constant (8.314×10^7 erg/mol), $\bar{\nu}$ is the partial specific volume (cubic centimeters per gram), and ρ is the solvent density (grams per cubic centimeter). The buffer density (1.00848 g/cm^3) was calculated from tabulated data.

The partial specific volume of M-TTR was estimated to be 0.7316 cm^3/g, based upon the amino acid composition.

Samples used to test a small molecule (Flu and DBF) or RBP−A binding to M-TTR were incubated at 37 °C for 2 h before the sedimentation velocity runs. For the RBP−A binding, samples were monitored at 330 nm using a partial specific volume of 0.73 cm^3/g for the data fitting.

Crystal Structure of M-TTR. M-TTR (12 mg/mL) was mixed in a 1:1 ratio with buffer solution 6 [0.2 M $MgCl_2$, 0.1 M Tris buffer (pH 8.5), and 30% (w/v) polyethylene glycol 4000] from crystal screen 1 (Hampton research) and covered with a drop of Al's oil. Crystals formed (0.2 mm × 0.2 mm × 0.1 mm) in 2−3 days at room temperature. The crystals were then placed in a cryoprotectant composed of 0.16 M $MgCl_2$, 0.08 M Tris buffer (pH 8.5), 24% (w/v) polyethylene glycol 4000, and 20% (v/v) anhydrous glycerol and flash-frozen in a 120 K liquid nitrogen cryostream. A DIP2030 imaging plate system (MAC Science, Yokohama, Japan) coupled to an RU200 rotating anode X-ray generator was used for data collection. Data were reduced with DENZO and SCALEPACK. The SCALEPACK file was next converted to an MTZ file for further processing using CCP4.

Denaturation Studies Monitoring Tryptophan Fluorescence. Fluorescence experiments were performed employing an Aviv (Lakewood, NJ) model ATF105 spectrofluorometer. Samples were excited at 295 nm with a bandwidth of 1 nm for 0.1 mg/mL samples and 2 nm for 0.01 mg/mL samples, whereas fluorescence emission spectra were recorded from 310 to 410 nm with a bandwidth of 6 nm. TTR (0.01 mg/mL, pH 7) was subjected to chemical denaturation (25 °C); samples were incubated in urea or GdnHCl for 24 (M-TTR) or 96 h (WT TTR) before data collection. Incubation in urea beyond 96 h was avoided since it will lead to excessive covalent modification of the protein samples. Renaturation samples (0.4 mg/mL) were incubated in either 9 M urea or 7.5 M GdnHCl for 96 h before dilution to the desired denaturant and TTR concentration (0.01 mg/mL). Diluted samples were incubated at 25 °C for 24 h before data collection. The ratio between the fluorescence intensity at 355 (exposed Trp) and 335 nm (buried Trp) was used to asses the extent of protein denaturation. The F_{355}/F_{335} ratio ranges from 0.8 to 1.3 for solvent-excluded (folded) and totally exposed (denatured) tryptophan residues, respectively. In cases where the fluorescence intensity changes dramatically (pH-induced denaturation), the global fluorescence was calculated using the following equation and the value was used to assess the extent of denaturation:

$$\text{global fluorescence} = \frac{\sum(F_i\lambda_i)}{\sum F_i} \qquad (2)$$

where F_i is the fluorescence intensity at wavelength λ_i, which ranges from 310 to 410 nm with 1 nm intervals.

Circular Dichroism Spectroscopy. The CD spectra of TTR were recorded on an Aviv model 202SF spectrometer. Far-UV CD experiments (200−250 nm) were carried out with 0.1 mg/mL TTR samples (pH 7) using a 2 mm quartz cuvette, while 0.4−0.6 mg/mL samples were used for near-UV experiments (250−320 nm), using a 10 mm path length cell.

Fibril Formation Assay. A TTR stock solution [in 10 mM sodium phosphate, 100 mM KCl, and 1 mM EDTA (pH 7)] was diluted 1:1 with 200 mM buffer as well as 100 mM KCl and 1 mM EDTA at the pH of interest to obtain solutions with the desired TTR concentration. Citrate buffer was used when a final pH of ≤3.4 was desired; phosphate buffer was employed for evaluating amyloidogenesis at pH 6.2 and 7.0, and acetate buffer was used when the pH was between 3.8 and 5.8. The influence of small molecule inhibitors (64.8 μM Flu or DBF) was evaluated by adding them to a 0.4 mg/mL TTR solution which was incubated for 2 h (37 °C) before the pH was dropped to 4.4 via a 1:1 dilution (acetate buffer). All fibril formation samples were further incubated at 37 °C for 72 h without stirring, except when time course data were collected, where samples were mixed and evaluated as a function of time at 37 °C with slight stirring. The extent of fibril formation was probed by turbidity measurements at 400 nm on an HP 845x UV−visible spectrometer equipped with a Peltier temperature-controlled cell holder. Single-time point samples (72 h) were vortexed immediately before the measurement.

Thioflavin T (TFT) binding to M-TTR was also used to follow amyloid fibril formation at pH 4.4. For each sample, a 25 μL aliquot (sample vortexed to ensure a homogeneous suspension) was taken out and mixed with pH 8 buffer (50 mM Tris, 100 mM KCl, and 1 mM EDTA), together with 2 μL of a TFT stock (1 mM) to reach a final volume of 200 μL with a final TFT concentration of 10 μM. The mixture was then excited at 440 nm, and the fluorescence emission intensity at 482 nm was recorded.

ANS Binding. The binding of ANS to TTR was performed in TTR solutions (0.1 mg/mL) containing 100 μM ANS. The excitation wavelength was set at 370 nm employing a bandwidth of 2 nm; emission spectra were recorded from 600 to 420 nm with a bandwidth of 6 nm.

Electron Microscopy. Long-term storage samples employed in the electron microscopy experiments were obtained by storing concentrated TTR solutions (>10 mg/mL) in pH 7 buffer at 4 °C for more than 2 weeks. The solution was then subjected to analytical size-exclusion chromatography using a Superdex75 column; soluble aggregates from the elution were collected and buffer exchanged with 50 mM phosphate, 100 mM KCl, and 1 mM EDTA. EM samples on fibrils formed under acidic conditions (pH 4.4) were taken from the fibril formation assay containing 0.2 mg/mL M-TTR. EM samples were prepared on a glow-discharged carbon-coated grid and stained with uranyl acetate. A Phillips CM-100 electron microscope was used to examine the grids. All electron micrographs were taken at 80−100 kV.

RESULTS

Design of a Monomeric Variant of Transthyretin (TTR). It is presumed that the conformational preferences of the F87M and L110M mutations on the two H−H′ β-sheet interfaces and the two AB−GH loop interfaces, respectively, hinder tetramer formation by the steric requirements of the Met side chain. Phe87 is positioned at the beginning of the F strand (directly below the H strand in the tertiary structure), whereas Leu110 is at the end of strand G, proximal to the hydrophobic interface mediated by the GH loop (Figure 1). Both residues have side chains pointing toward neighboring subunits, hence the presumed steric impediment to quaternary structure formation. These semiconservative hydrophobic

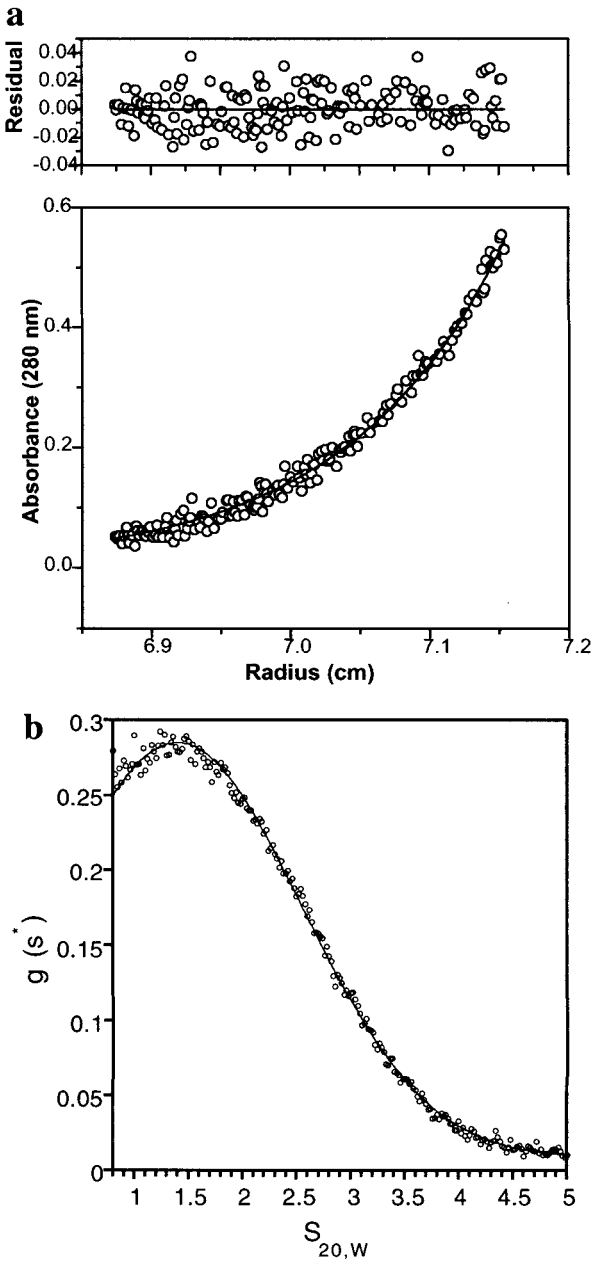

FIGURE 2: (a) Sedimentation equilibrium analysis of M-TTR (0.4 mg/mL). The solid line is the fitting result employing a single-ideal species model using a nonlinear least-squares analysis with the Origin software and fitting to the experimental data (○). The random residuals (difference between experimental and fitted data) are shown in the top panel. (b) Sedimentation coefficient distribution of M-TTR (0.4 mg/mL) determined by a sedimentation velocity experiment. The solid line represents the single-species fit to the experimental data (○) using the DCDT+ program (*44*).

replacements are not likely to dramatically alter the conformation of the monomer or interfere with the aberrant self-assembly process required for TTR amyloid fibril formation.

Quaternary Structure of F87M/L110M (M-TTR) or Lack Thereof. Analytical ultracentrifugation analysis and gel filtration chromatography were employed to characterize the quaternary structure (or lack thereof) of the recombinant Phe87Met/Leu110Met TTR variant (M-TTR). The M-TTR variant (28.8 μM) was subjected to both equilibrium and velocity analytical ultracentrifugation studies at 20 °C (Figure 2). The equilibrium data fit very well to a single-ideal species model, yielding a MW of 13.81 ± 0.31 kDa, in excellent

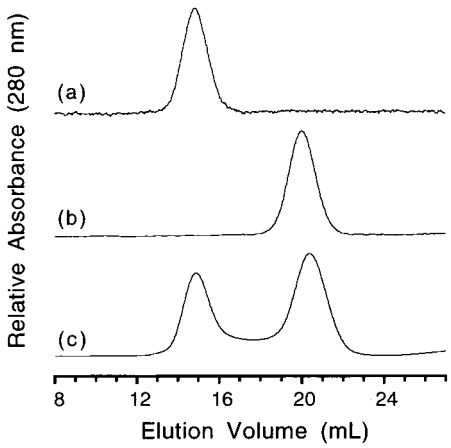

FIGURE 3: Analytical size-exclusion chromatographs of 0.1 mg/mL (pH 7) samples of (a) WT TTR, (b) M-TTR, and (c) F87M TTR.

agreement with the expected MW (13.89 kDa) of a TTR monomer. The residuals (difference between the experimental data and the fit dictated by eq 1) are small and random, demonstrating the appropriateness of the model. The sedimentation velocity data afford a sedimentation coefficient ($S_{20,w}$) of 1.45 S, corresponding to a MW of 13.18 ± 0.1 kDa, consistent with a monomeric structure (Figure 2b). Previous velocity studies on TTR monomers produced by denaturing conditions provide a range of sedimentation coefficients ($S_{20,w}$ = 1.2−1.8 S) flanking the value observed for M-TTR (*24*). The analytical ultracentrifugation experiments demonstrate that M-TTR is ≥95% monomeric in solution over a concentration range of 7.2 μM to 0.1 mM; in fact, no tetramer can be detected.

Three TTR quaternary structures can be resolved by Superdex 75 analytical gel filtration chromatography: the tetramer, the monomer, and high-molecular mass soluble oligomers (MW > 2 million Da). These bands were assigned through calibration using MW standards and the assignments verified by performing analytical ultracentrifugation studies on the collected fractions. At neutral pH, freshly purified WT TTR and the M-TTR variant elute exclusively as a tetramer and monomer, respectively (Figure 3a,b). To make sure that the coexistence of tetramer and monomer could be detected chromatographically, we characterized the F87M TTR variant previously demonstrated to be a mixture of tetramer and monomer by analytical ultracentrifugation analysis. The F87M TTR variant eluted from the column as two peaks, consistent with the retention time of tetramer and monomer, respectively (Figure 3c). Electrospray LC−MS analysis confirmed that both peaks are full-length F87M TTR. The Stokes radius (R_S) was estimated to be 19.5 and 32.3 Å for M-TTR and WT TTR, respectively, based on a calibration curve generated from a set of global proteins with known R_S values, using standard procedures (*28*).

Since TTR subunits are a component of a quaternary structure comprised of as many as 10 molecules [4 mol of TTR, 2 mol of thyroid hormone or a thyroid mimetic, and 2 mol of the 21 kDa retinol binding protein−vitamin A complex (RBP−A)] in human plasma, it was desirable to test whether it would be possible to make monomeric M-TTR assemble into a tetramer by adding its binding partners. Flufenamic acid (Flu) and 4,6-dibenzofurandicarboxylic acid (DBF) are thyroid mimics that bind to tetrameric TTR with

a nanomolar dissociation constant. These small molecules are known to inhibit TTR amyloid fibril formation through a tetramer stabilization mechanism (*29*, *30*). While less than 10% of the M-TTR (28.8 μM) forms a tetrameric quaternary structure in the presence of 14.4 μM Flu or DBF, ~50% of the protein adopted a tetrameric quaternary structure when the small molecule concentration was increased to 64.8 μM, based on sedimentation velocity analyses. This demonstrates that an appropriate ligand can shift the equilibrium toward the tetramer, providing further evidence of the efficacy of these small molecule inhibitors as tetramer stabilizers.

Monomeric M-TTR (36 $\mu M_{monomer}$, 0.5 mg/mL) is shifted to a tetrameric TTR quaternary structure when mixed with RBP−A (9 μM). The dominant species detected by sedimentation velocity studies has a $S_{20,w}$ value of 4.86 corresponding to a MW of 68.0 ± 0.5 kDa (data not shown), consistent with a protein complex made up of one RBP molecule and four subunits of M-TTR. The crystal structure of the $(RBP-A)_2$·WT TTR complex reveals extensive surface contacts between the two proteins; in fact, each RBP is in contact with three different subunits in the WT TTR tetramer (*31*, *32*). Therefore, it is not surprising that RBP can induce M-TTR to adopt a tetrameric quaternary structure.

Recently, we discovered that anions, including Cl^-, are able to bind to the TTR tetramer (*45*), dramatically stabilizing this quaternary structure. While a buffer containing 1.5 M Cl^- was capable of saturating the Cl^- interaction sites in the tetrameric TTR, rendering the protein nonamyloidogenic (pH 4.4) and not denaturable by urea, anion binding was unable to shift M-TTR to a tetramer, based on a sedimentation velocity analysis (data not shown).

Secondary and Tertiary Structures of M-TTR Relative to WT TTR. The circular dichroism (CD) spectrum of monomeric M-TTR is virtually identical to that exhibited by tetrameric WT TTR, the 215 nm minimum being typical of a protein having a predominant β-sheet rich secondary structure (Figure 4a). The fluorescence emission spectra are also nearly identical (Figure 4b). The 1D proton NMR spectrum of M-TTR has chemical shift dispersion very similar to that exhibited by the WT tetramer possessing 2,2,2 molecular symmetry (Figure 4c). The far-UV CD, fluorescence, and 1D proton NMR spectral similarities suggest that the secondary and tertiary structures in M-TTR and WT TTR are very similar if not identical.

1-Anilino-8-naphthalenesulfonate (ANS) is a commonly used fluorescent probe for detecting solvent-exposed hydrophobic residues in proteins (*33*). While folded proteins do not typically bind ANS, tetrameric WT TTR binds 2 equiv of ANS in its thyroid hormone binding channel, enhancing ANS fluorescence intensity (Figure 5). Unlike the WT tetramer, M-TTR does not bind ANS at pH 7, consistent with a folded structure lacking exposed hydrophobic surface area. The inability of ANS to dramatically shift monomeric M-TTR to a tetramer is clear.

Crystal Structure of M-TTR. Crystals of M-TTR belong to space group $P2_12_12_1$ with four M-TTR subunits (two dimers) in each asymmetric unit with the following unit cell dimensions: $a = 64.73$ Å, $b = 83.30$ Å, and $c = 88.13$ Å. This is different from the WT TTR crystal which has a $P2_12_12$ space group (*29*). The crystallographic *R*-factor of M-TTR was refined to 22% for all reflections between 12 and 2.1 Å, with an R_{free} of 27.55% (Protein Data Bank entry 1gko). The M-TTR model has a root-mean-square deviation from ideal protein geometry in bond length of 0.010 Å and bond angle distances of 1.54 Å. A PROCHECK calculation shows that all main chain dihedral angles are in the allowed regions. Overall, the solution of the X-ray crystal structure of M-TTR reveals that its tertiary structure is nearly identical to that of WT TTR (Figure 6), confirming the results presented above. It is interesting that M-TTR crystallizes as a tetramer. However, it is not surprising given the high concentrations reached in the precipitant and the very similar M-TTR and WT TTR tertiary structures.

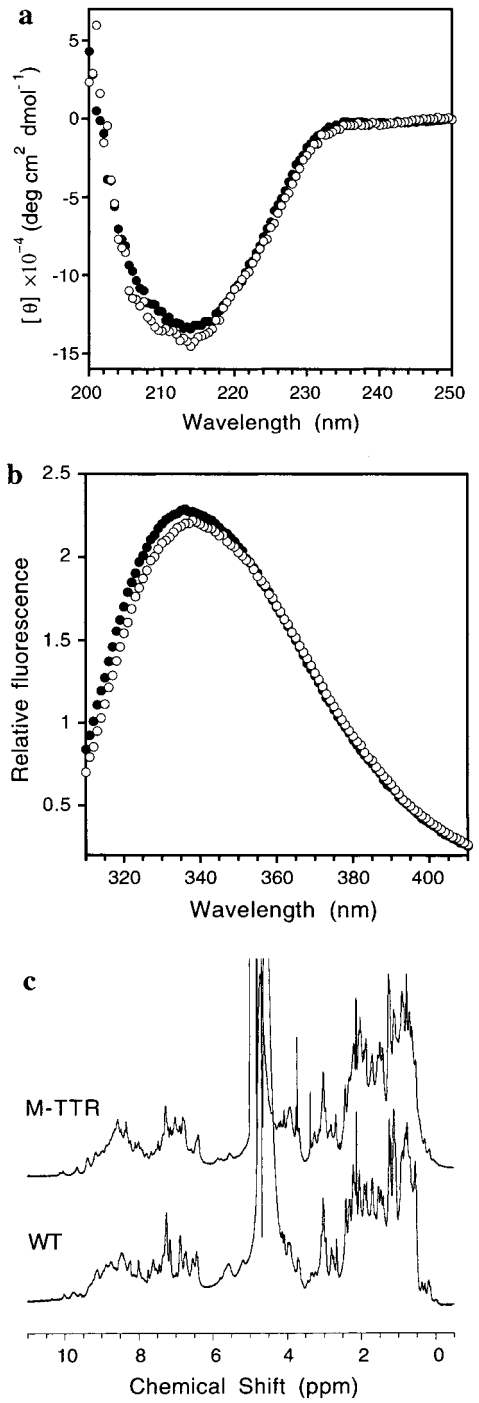

FIGURE 4: Spectroscopic comparisons of M-TTR and WT TTR. (a) Far-UV CD spectra and (b) Trp fluorescence emission scans for 0.1 mg/mL M-TTR (●) and the WT TTR (○) at 25 °C. (c) 1D proton NMR spectra of M-TTR (top) and WT TTR (bottom).

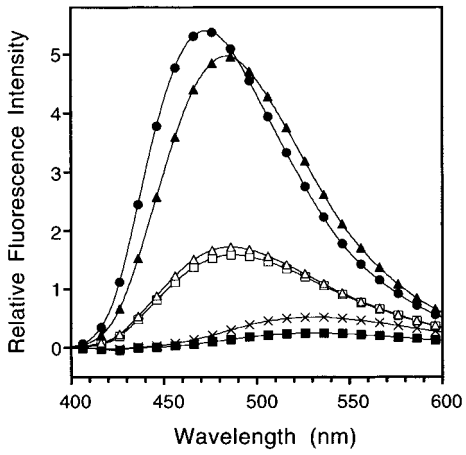

FIGURE 5: Fluorescence emission spectra of 100 μM ANS in pH 7 buffer (×), in the presence of 0.1 mg/mL WT at pH 7 (●), in the presence of 0.1 mg/mL M-TTR at pH 7 (■), 4.4 (△), and 3.6 (▲), and in the presence of M-TTR after long-term storage (□). Samples were excited at 370 nm.

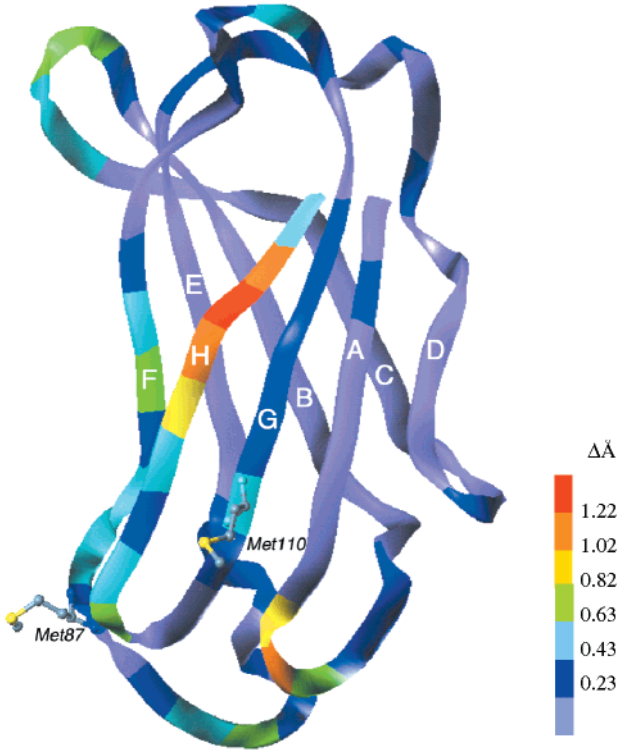

FIGURE 6: Ribbon diagram of chain A from the crystal structure of M-TTR (PDB entry 1gko). The color coding indicates the deviation of C_α atoms relative to the WT TTR structure.

Subtle differences are observed when comparing M-TTR and WT TTR crystal structures, with backbone C_α atoms deviating from 0.2 to 1.4 Å. It is clear from Figure 6 that most of the deviations are observed on strands F, G, and H and on the interfaces between the subunits. This is consistent with the design of M-TTR where the interfaces are destabilized. Moreover, almost all the loops between the strands exhibit obvious deviations. Interestingly, heterogeneity is exhibited when comparing subunit A (identical to subunit C) and subunit B (identical to subunit D) in the M-TTR crystal structure, especially in the FG loop region. While the FG loop in the A or C subunit of M-TTR can be superimposed with that of WT TTR, that in the B or D subunit resembles the FG loop in L55P TTR and cannot be superimposed with the conformation exhibited by WT TTR (*22*, *34*).

The tetrameric crystal structure of M-TTR as well as the conformational heterogeneity exhibited when comparing subunits within the tetramer may be a reflection of the existence of a "crystallization artifact", i.e., the observation of quaternary structure that is not populated in solution due to protein−protein contacts within the crystal lattice. It is conceivable that such an artifact may also mask differences between TTR mutants, providing a putative explanation for why so many variants, amyloid-forming and non-amyloid-forming alike, do not exhibit significant structural differences (*22*). On the other hand, the fact that M-TTR crystallizes in a different space group than WT indicates that the altered conformation of the FG loop region is significant.

Folding Thermodynamics of M-TTR Relative to WT TTR. Trp fluorescence was used to monitor GdnHCl and urea-induced denaturation of M-TTR. There are two tryptophan residues in TTR, Trp-41 and Trp-79 (the latter is quenched in the folded state) (*35*). In WT TTR and M-TTR, the Trp fluorescence exhibits a red shift (from 337 to 358 nm) and an intensity increase upon chaotrope denaturation (Figure 7a). GdnHCl denaturation and reconstitution of WT TTR have been reported previously (*23*). Dramatic hysteresis was observed when comparing the GdnHCl denaturation curves to dilution-induced refolding curves where the midpoints of denaturation and reconstitution are >5 and <2 M, respectively (Figure 7b). C_2 symmetric anion interaction sites in the WT TTR tetramer account for the dramatic hysteresis observed in ionic denaturants (*45*). Since Cl^- ion binding stabilizes the protein, counteracting the guanidinium ion during denaturation, it seems reasonable that the refolding curve (with a midpoint at <2 M GdnHCl) represents the "true" stability of the WT TTR tertiary structure. Urea-mediated denaturation of WT TTR (≤0.1 mg/mL) is reversible (Figure 7c), although the approach to equilibrium under unfolding conditions is very slow (days), particularly at high TTR concentrations. The urea denaturation curves for WT TTR are concentration-independent in the 0.01−0.1 mg/mL range. This indicates that the tetramer−monomer preequilibrium apparently required for denaturation by urea is not detected by Trp fluorescence, consistent with data shown in Figure 4b that indicate indistinguishable Trp fluorescence emission scans for M-TTR and WT TTR. The urea denaturation curves are recorded in the presence of 100 mM KCl and 50 mM sodium phosphate buffer (pH 7) unless otherwise noted.

The urea- and GdnHCl-induced denaturation- and dilution-induced refolding curves for M-TTR exhibit fully reversible and highly cooperative transitions. The GdnHCl-induced denaturation of M-TTR (Figure 7b) relative to that of urea (Figure 7c) occurs at a much lower chaotrope concentration in keeping with the known potency of GdnHCl, consistent with the expectation that the monomeric structure of M-TTR is incapable of taking advantage of the Cl^--induced stabilization available to the WT tetramer. Even though the urea-induced denaturation curves of M-TTR and WT TTR are almost identical, the approach to equilibrium is dramatically faster for M-TTR. Stopped-flow experiments show that the half-life of unfolding and folding for M-TTR is between 10 and 200 ms in both urea and GdnHCl (detailed kinetic studies will be published elsewhere), compared to the much longer

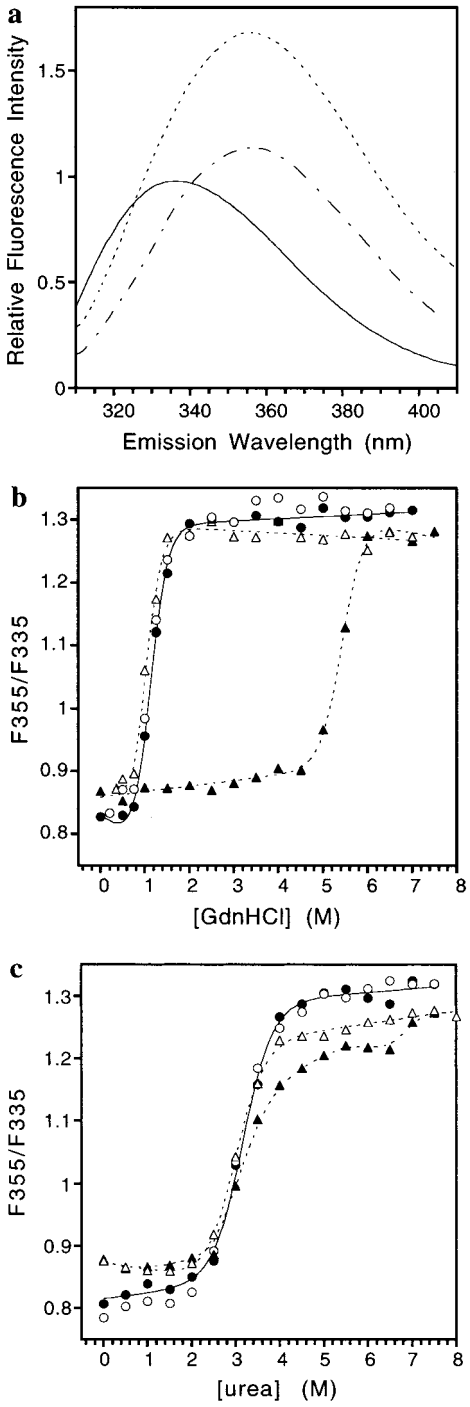

FIGURE 7: Trp fluorescence-monitored GdnHCl and urea denaturation of M-TTR and WT TTR. All samples were incubated for 24 h at room temperature before analysis. Emission spectra were collected at 25 °C on 0.01 mg/mL protein solutions; samples were excited at 295 nm. (a) Emission spectra of M-TTR with 0 M denaturant (—), 7 M GdnHCl (—·—), and 7.5 M urea (- - -). (b) GdnHCl- and (c) urea-induced denaturation curves (blackened symbols) and refolding (open symbols) of M-TTR (circles) and WT TTR (triangles), created by plotting the ratio between fluorescence intensity at 355 and 335 nm as a function of denaturant concentration. Solid lines through the M-TTR denaturation data are fitted to a two-state model, while the dotted lines through the WT data are smoothed curves to facilitate viewing.

periods required to denature tetrameric WT TTR (days), as a result of slow tetramer dissociation. When fitted to a two-state model, M-TTR exhibits a ΔG_u value of 5.5 ± 0.8 kcal mol^{-1} and an *m* value of 1.7 ± 0.2 kcal mol^{-1} M^{-1} in urea;

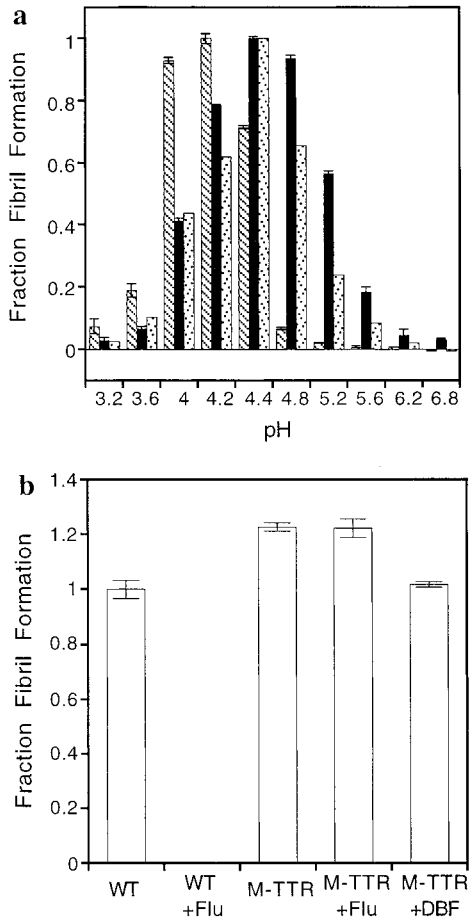

FIGURE 8: Fibril formation of M-TTR and WT TTR (0.2 mg/mL) as a function of pH. The *y*-axis is the fraction of fibril formation determined by turbidity at 400 nm (M-TTR and WT TTR) and thioflavin T binding (M-TTR). Samples were incubated at 37 °C for 72 h before the assay. (a) M-TTR and WT TTR amyloidogenicities probed by turbidity are represented by black and hatched bars, respectively, while data from TFT binding probing M-TTR amyloid formation are represented by dotted bars. (b) Small molecule TTR inhibitors, Flu and DBF, do not inhibit fibril formation of M-TTR at pH 4.4 and 37 °C.

whereas in GdnHCl, the values are 3.4 ± 0.4 kcal mol^{-1} and 3.1 ± 0.3 kcal mol^{-1} M^{-1}, respectively.

M-TTR Amyloidogenicity. The M-TTR variant does not form fibrils spontaneously at neutral pH, even at a concentration as high as 15 mg/mL (1 mM) over a period of several days when stored at 4 °C, demonstrating the necessity for partial denaturation. Tetrameric WT and monomeric M-TTR amyloidogenesis under acidic conditions was monitored by turbidity at 400 nm (M-TTR amyloidogenicity also quantified by thioflavin T binding) (Figure 8a). Electron microscopy and TFT binding confirm the amyloid-like structure of the assemblies of M-TTR formed at pH <6 (see below). The pH-dependent amyloidogenicities of WT TTR and M-TTR are similar, but not identical, M-TTR being able to self-assemble at slightly higher pH values and over a broader range, consistent with the absence of the tetramer−folded monomer preequilibrium that influences WT behavior. For example, 0.2 mg/mL M-TTR forms amyloid fibrils at pH >5 unlike the WT tetramer which cannot efficiently dissociate to the amyloidogenic intermediate until a pH of <5 is reached (*35*, *36*).

Fibril formation from WT TTR can be completely inhibited by adding 2 equiv of small molecule inhibitors such

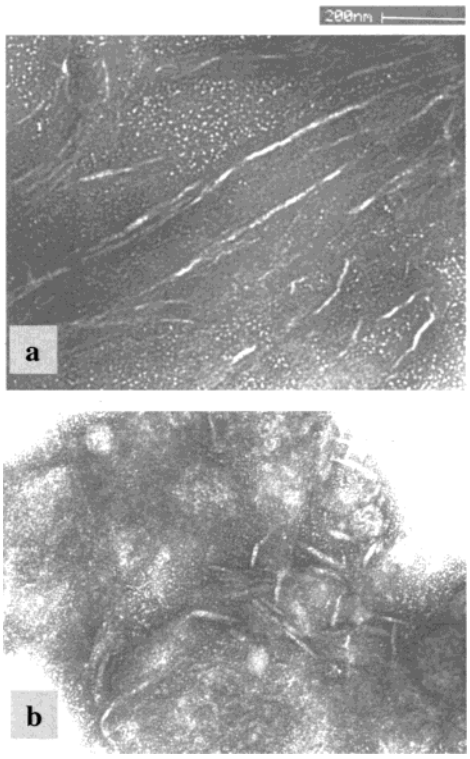

FIGURE 9: Electron microscopic images of M-TTR samples made from (a) 0.2 mg/mL M-TTR incubated at 37 °C for 72 h at pH 4.4 in acetate buffer. (b) Soluble aggregates isolated from a 15 mg/mL sample stored in 10 mM Tris buffer at pH 7.4 and 4 °C for 3 weeks. The scale bar is 200 nm.

as Flu and DBF (*29*, *30*); RBP binding also modestly inhibits WT TTR fibril formation (J. White et al., unpublished results). The mechanism of both types of inhibition is by tetramer stabilization. Even though analytical ultracentrifugation analysis demonstrates tetramer formation of M-TTR upon addition of RBP or thyroxine mimics at concentrations above physiological, addition of the ligands at 2-fold the physiological concentration does not significantly inhibit M-TTR fibril formation, judged by either the amount of fibrils formed or the rate at which the fibrils form (Figure 8b). This could simply be a reflection of the intrinsically unstable tetrameric structure formed by M-TTR, even in the presence of the ligands.

Electron microscopy (EM) was utilized to evaluate the products of M-TTR self-assembly. Studies have shown that the most pathogenic variant, L55P, forms fibrils at low pH and protofilaments under physiological conditions upon long-term storage (*27*). Electron microscopy evaluation demonstrates that M-TTR forms mature fibrils at pH 4.4 (Figure 9a), while soluble aggregates formed from M-TTR after long-term storage at 4 °C are filaments (Figure 9b). Filaments may or may not be on the pathway toward mature fibril formation.

Kinetics of M-TTR Amyloid Fibril Formation. Since the rate-determining step of WT TTR amyloid fibril formation appears to be tetramer dissociation, we expected a dramatic difference in comparing its rate to that of monomeric M-TTR. At pH 4.4 (37 °C), where both M-TTR and WT TTR exhibit a near-maximal yield of fibrils, the M-TTR variant forms fibril much faster than the WT (Figure 10). While the time course of WT TTR (0.2 mg/mL) amyloidogenesis requires 72 h to plateau ($t_{1/2} \approx 15$ h) (*35*), M-TTR fibrillization is

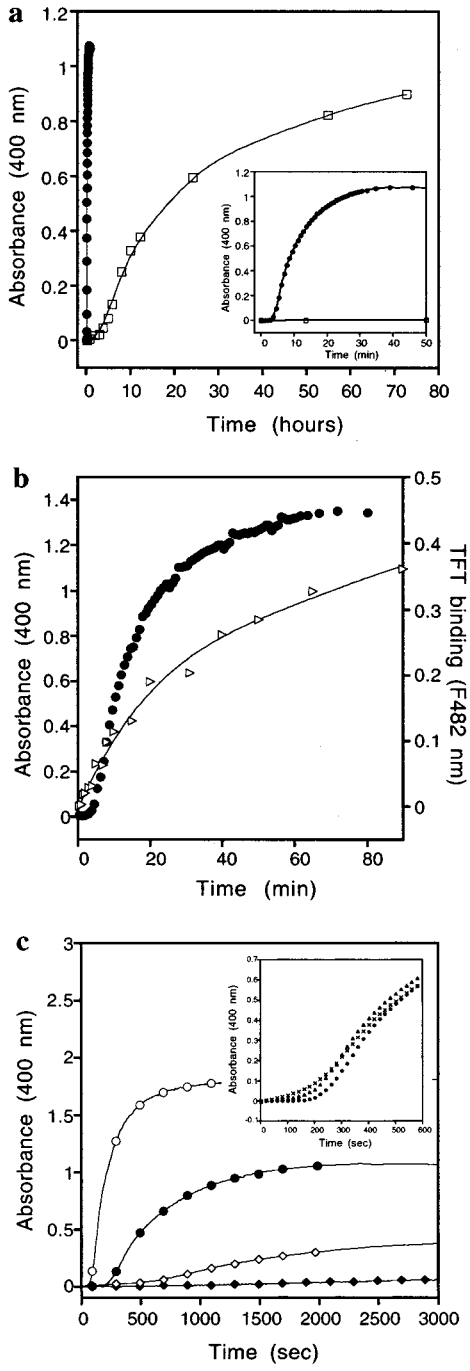

FIGURE 10: Time course of TTR self-assembly into fibrils at pH 4.4 (37 °C). (a) Comparison of the turbidity changes (400 nm) for M-TTR (●) and WT TTR (□) (0.2 mg/mL) as a function of time. The inset is a blowup of the M-TTR time course for the first 50 min. (b) M-TTR (0.2 mg/mL) fibril formation monitored by both turbidity at 400 nm (●) and TFT binding using fluorescence emission intensity at 482 nm (tilted triangle). The maximum turbidity and fluorescence values this sample can reach (after incubation for 72 h at 37 °C) are 1.4 and 0.9, respectively. (c) Concentration-dependent fibril formation of M-TTR at 0.4 (○), 0.2 (●), 0.1 (◇), and 0.05 mg/mL (◆). The inset compares 0.2 mg/mL M-TTR without seeding (●) or seeded with 2% M-TTR (×) and WT (△) fibrils. Solid lines are the real data, and symbols represent 10% of the data points.

completed within 1 h ($t_{1/2} \approx 12$ min) (Figure 10a). Monomeric M-TTR amyloidogenesis detected by TFT binding is slightly slower (Figure 10b). Interestingly, amyloidogenesis detected by TFT binding does not indicate any sign of lag phase, suggesting fibrillization is instantaneous. This cannot

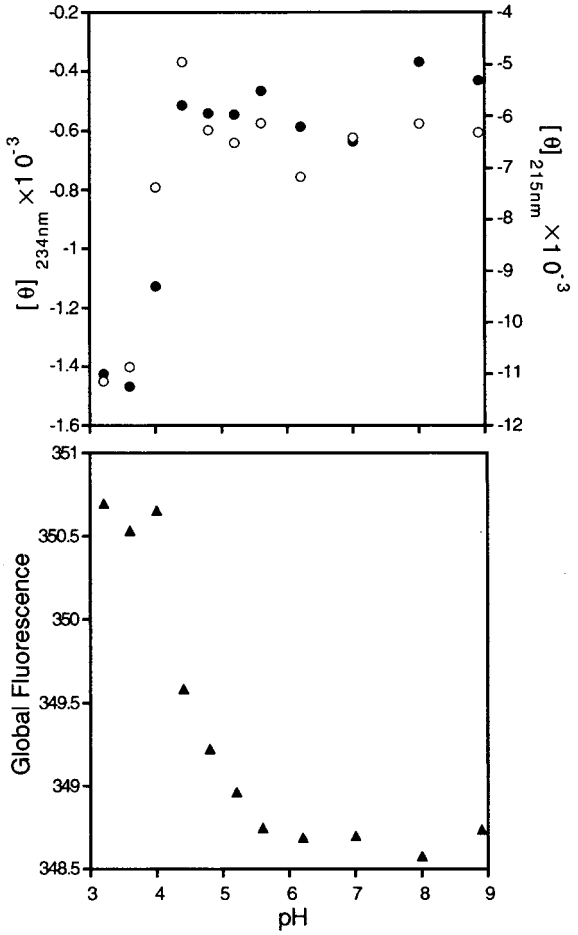

FIGURE 11: pH-dependent structural changes of M-TTR monitored by far-UV CD molar ellipticity (degress per square centimeter per decimole) at 234 (●) and 215 nm (○) (top panel). The bottom panel illustrates pH-dependent tertiary structural changes monitored by Trp fluorescence (▲). The pH 4.4 data point may have a contribution from high-molecular mass soluble aggregates.

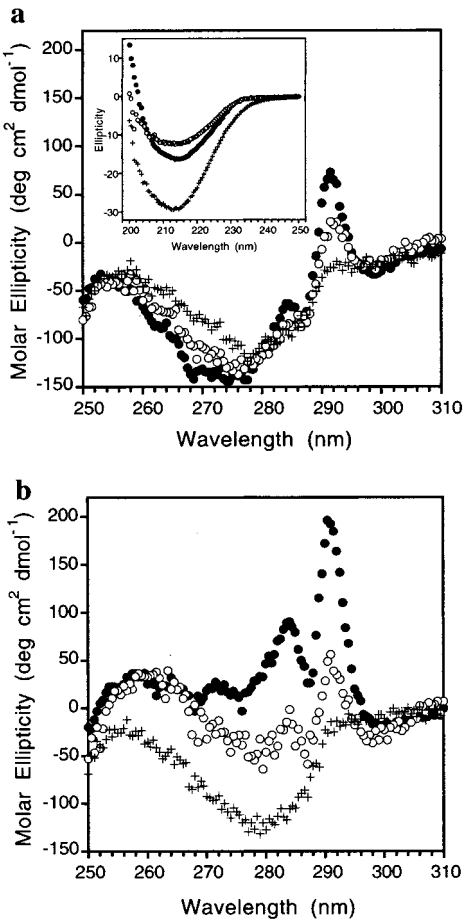

FIGURE 12: Near-UV CD scans of 0.4−0.55 mg/mL M-TTR (a) and WT TTR (b) at pH 7 (●), 4.4 (○), and 3.6 (+). The inset in panel a shows the far-UV CD scans of 0.1 mg/mL M-TTR at the same pH values.

be discerned by turbidity because the particles are not large enough to scatter light at $t < 3$ mins.

M-TTR but Not WT TTR Amyloid Fibril Formation Is Seedable. Previous attempts at seeding WT TTR amyloid fibril formation were not successful, presumably due to the fact that tetramer dissociation is the rate-determining step, not fibril growth (*35*). However, the rate-determining step should change for M-TTR, and in fact, M-TTR is susceptible to a rate increase by seeding by either M-TTR or WT TTR fibrils (inset of Figure 10c). Furthermore, the initial rate of fibril formation increases dramatically with M-TTR concentration, accompanied by the shortening of the lag phase with increasing concentration (Figure 10c).

M-TTR pH-Dependent Structural Changes Are Required for Amyloidogenicity. The pH-dependent structural changes enabling M-TTR to form fibrils were studied using CD and fluorescence spectroscopy. Over the pH range of 9−6, M-TTR adopts a native structure according to far-UV CD and Trp fluorescence measurements, consistent with its inability to efficiently form amyloid fibrils (Figure 8a). A transition is observed at pH <6 by fluorescence (tertiary structure) and pH <5 by far-UV CD (secondary structure) (all spectra were recorded at 25 °C where there is little or no fibril formation) (Figure 11). Fibril formation at 37 °C is easily observed at pH <6 and becomes very efficient at pH <5, indicating that fluoresence is more sensitive to the conformational changes leading to the formation of the amyloidogenic intermediate than is far-UV CD. When the pH is reduced to <4, M-TTR forms an alternative conformation with higher β-sheet content and maximally exposed tryptophan residues that is less amyloidogenic (Figures 8a, 11, and 12).

Near-UV CD studies were also employed to evaluate pH-dependent tertiary structural changes (Figure 12). Over the pH range where TTR is not amyloidogenic (pH 7.5−5.0), WT TTR exhibits two maxima at 283 and 291 nm (Figure 12b) (*35*). The intensities of these maxima decrease as the pH is reduced to the range where the monomeric amyloidogenic intermediate is produced (pH 4−5). As the pH is reduced to <4, a broad negative peak centered ∼278 nm appears at the expense of the two maxima, eventually becoming the dominant signal at pH 2−3 (*35*) (Figure 12b). The near-UV CD spectra of 0.4−0.6 mg/mL M-TTR at pH 7 (25 °C) exhibit the maxima of the WT spectra as well as a broad minimum ∼270−276 nm (Figure 12a). The characteristic positive peaks indicate that M-TTR and the monomeric subunit in the WT tetramer exhibit similar tertiary structures. The broad negative peak is likely a result of the fact the M-TTR does not assemble into a tetramer and thus has a different environment around some of the Trp and Tyr residues. Nevertheless, under acidic conditions, both M-TTR and the WT TTR [previously shown to be predominantly

monomeric at pH 4.4 (*1*)] go through very similar if not identical tertiary structural changes based on spectral similarities, indicating very similar amyloidogenic tertiary structures. While ANS does not bind to M-TTR at pH 7, it does bind over the amyloid-forming range (e.g., at pH 4.4), indicating an increased level of exposure of hydrophobic surface, consistent with the pH-dependent tertiary structural changes. At pH 3.6, ANS strongly binds to M-TTR (increased fluorescence intensity and a blue shift in the emission maximum), characteristic of a molten globular structure that is dramatically less amyloidogenic (Figure 5). The increased secondary structural content and lack of a rigid tertiary structure exhibited by TTR at such low pH (Figure 12a) are also typical of a molten globule conformation (*37*, *38*).

DISCUSSION

Folded Monomeric M-TTR Is Not Amyloidogenic; However, pH-Mediated Partial Denaturation Leads to Fibril Formation. M-TTR adopts a monomeric structure in aqueous solution according to analytical equilibrium ultracentrifugation and gel filtration studies. The monomer and tetramer appear to be in equilibrium, although the tetramer concentration is so low that it is not observable unless an appropriate tetramer-binding ligand is added. The equilibrium can be shifted toward the tetramer by adding small molecule inhibitors (thyroxine mimics) or retinol binding protein, albeit at concentrations of protein and ligand slightly above those that are physiologically relevant. We interpret this to mean that M-TTR has a monomeric native tertiary structure (confirmed by NMR and fluorescence studies) that can be driven to self-assemble by adding ligands or crystallizing the protein at high concentrations (M-TTR crystallizes as a tetramer). The monomer can form amorphous aggregates after long-term storage at neutral pH; however, M-TTR does not spontaneously form fibrils on a biologically relevant time scale ($t_{1/2}$ = 8−18 h) at pH 7. Thus, the normally folded TTR monomer is not amyloidogenic. The very low yield of unstructured aggregates formed after a lengthy incubation period likely arises from the equilibrium ratio between the folded and unfolded state that may be as low as 1000:1. Irrespective of whether a distinction is made between the fibrillar aggregates formed under acidic conditions or amorphous aggregates inefficiently formed after extended incubation at neutral pH, it is clear that aggregation is much more efficient at low pH (Figure 8). Efficient fibril formation under slightly acidic conditions is mediated by a tertiary structural change that can be detected by fluorescence as well as by near-UV CD methods. The acid-mediated M-TTR tertiary structural changes are strictly analogous to what was seen for tetrameric WT TTR (*35*). Hence, the species that forms amyloid efficiently on a biologically relevant time scale is an alternatively folded monomer. By extension, these data strongly suggest that WT tetramer dissociation in the absence of conformational changes is necessary but not sufficient for amyloid fibril formation.

The Tetramer to Monomer to Alternatively Folded Monomer Linked Equilibria Strongly Influence Amyloidogenicity. At pH 4.4, M-TTR forms amyloid fibrils more than 100 times faster than WT TTR (Figure 10a). Amyloidogenesis of the former but not the latter is seedable. This is consistent with the fact that tetrameric TTR dissociation is the rate-limiting step when WT TTR is converted to fibrils by an acid-mediated denaturation mechanism; hence, seeding which speeds up nucleation has no effect (*39*), whereas seeding enhances the rate of M-TTR fibrillization because nucleus formation is now one of the rate-limiting steps.

Ligands that enhance TTR tetramer stability shift the tetramer to folded monomer equilibrium toward tetramer and likely increase the activation barrier of dissociation and thus slow the rate of folded monomer production, required but not sufficient for fibril formation. The kinetics of fibrillization of M-TTR are much faster because the tetramer to folded monomer preequilibrium does not play a role. This preequilibrium has a significant kinetic barrier associated with it, evident from subunit exchange experiments recently published (*40*). The rate is strongly influenced by ions, and small and macromolecular ligands.

Is Monomeric TTR Accumulation Responsible for Fibril Formation in Vivo? Some in vitro studies based on gel filtration-isolated monomeric WT, V30M, and L55P TTR suggest that the monomer is not in equilibrium with the tetramer (*41*, *42*); however, it is necessary to exclude other reasons for this observation. The reversibility of unfolding and refolding (using urea, GdnHCl, and pH) of WT TTR and the demonstration that tagged and untagged WT TTR exchange subunits by a dissociative mechanism (presumably through the folded monomer) suggest that the monomer can reassemble into the tetramer (*40*). There may be circumstances where the tetramer and monomer are not at equilibrium because of modulation of the kinetic barriers associated with the tetramer to monomer equilibrium by other molecules and ions, and this is being further explored. It is clear that this issue is important because the accumulation of monomeric TTR in vivo is dangerous because of low kinetic barrier associated with its amyloidogenicity.

CONCLUSION

The discovery of a stable normally folded monomeric version of transthyretin is highly enabling in that it allows us to uncouple quaternary and tertiary structural changes associated with amyloidogenicity and to understand the kinetics and thermodynamics of denaturation and amyloidogenicity.

ACKNOWLEDGMENT

We are grateful to Drs. M. Jäger and E. Powers for helpful discussions and Dr. K. Liu and S. Deechongkit for their experimental expertise.

REFERENCES

1. Colon, W., and Kelly, J. W. (1992) *Biochemistry 31*, 8654−8660.
2. Kelly, J. W. (1996) *Curr. Opin. Struct. Biol. 6*, 11−17.
3. Kelly, J. W. (1998) *Curr. Opin. Struct. Biol. 8*, 101−106.
4. Stevens, F. J., Pokkuluri, P. R., and Schiffer, M. (2000) *Biochemistry 39*, 15291−15296.
5. Dobson, C. M. (1999) *Trends Biochem. Sci. 24*, 329−332.
6. Buxbaum, J. N., and Tagoe, C. E. (2000) *Annu. Rev. Med. 51*, 543−569.
7. Jimenez, J. L., Guijarro, J. I., Orlova, E., Zurdo, J., Dobson, C. M., Sunde, M., and Saibil, H. R. (1999) *EMBO J. 18*, 815−821.
8. Blake, C., and Serpell, L. (1996) *Structure 4*, 989−998.
9. Baldwin, M. A., Cohen, F. E., and Prusiner, S. B. (1995) *J. Biol. Chem. 270*, 119197−19200.

10. Booth, D. R., Sunde, M., Bellotti, V., Robinson, C. V., Hutchinsion, W. L., Fraser, P. E., Hawkins, P. N., Dobson, C. M., Radford, S. E., Blake, C. C. F., and Pepys, M. B. (1997) *Nature 385*, 787−793.
11. Uversky, V. N., Li, J., and Fink, A. L. (2001) *J. Biol. Chem. 276*, 10737−10744.
12. Liu, K., Cho, H. S., Lashuel, H. A., Kelly, J. W., and Wemmer, D. E. (2000) *Nat. Struct. Biol. 7*, 754−757.
13. Jackson, G. S., Hosszu, L. L. P., Power, A., Hill, A. F., Kenney, J., Saibil, H., Craven, C. J., Waltho, J. P., Clarke, A. R., and Collinge, J. (1999) *Science 283*, 1935−1937.
14. Guijarro, J. I., Sunde, M., Jones, J. A., Campbell, I. D., and Dobson, C. M. (1998) *Proc. Natl. Acad. Sci. U.S.A. 95*, 4224−4228.
15. Fandrich, M., Fletcher, M. A., and Dobson, C. M. (2001) *Nature 410*, 165−166.
16. Pertinhez, T. A., Bouchard, M., Tomlinson, E. J., Wain, R., Ferguson, S. J., Dobson, C. M., and Smith, L. J. (2001) *FEBS Lett. 495*, 184−186.
17. Damaschun, G., Damaschun, H., Fabian, H., Gast, K., Krober, R., Wieske, M., and Zirwer, D. (2000) *Proteins 39*, 204−211.
18. Konno, T., Murata, K., and Nagayama, K. (1999) *FEBS Lett. 454*, 122−126.
19. Westermark, P., Sletten, K., Johansson, B., and Cornwell, G. G., III (1990) *Proc. Natl. Acad. Sci. U.S.A. 87*, 2843−2845.
20. Saraiva, M. J. M., Birken, S., Costa, P. P., and Goodman, D. S. (1984) *J. Clin. Invest. 74*, 104−119.
21. McCutchen, S. L., Lai, A., Miroy, G. J., Kelly, J. W., and Colon, W. (1995) *Biochemistry 34*, 13527−13536.
22. Hornberg, A., Eneqvist, T., Olofsson, A., Lundgren, E., and Sauer-Eriksson, A. E. (2000) *J. Mol. Biol. 302*, 649−669.
23. Lai, Z., McCulloch, J., Lashuel, H. A., and Kelly, J. W. (1997) *Biochemistry 36*, 10230−10239.
24. Lashuel, H. A., Lai, Z., and Kelly, J. W. (1998) *Biochemistry 37*, 17851−17864.
25. Redondo, C., Admas, A. M., and Saraiva, M. J. M. (2000) *Biochem. J. 348*, 167−172.
26. Ferrao-Gonzales, A. D., Souto, S. O., Silva, J. L., and Foguel, D. (2000) *Proc. Natl. Acad. Sci. U.S.A. 97*, 6445−6450.
27. Lashuel, H. A., Wurth, C., Woo, L., and Kelly, J. W. (1999) *Biochemistry 38*, 13560−13573.
28. Uversky, V. N. (1993) *Biochemistry 32*, 13288−13298.
29. Peterson, S. A., Klabunde, T., Lashuel, H. A., Purkey, H., Sacchettini, J. C., and Kelly, J. W. (1998) *Proc. Natl. Acad. Sci. U.S.A. 95*, 12956−12960.
30. Klabunde, T., Petrassi, H. M., Oza, V. B., Raman, P., Kelly, J. W., and Sacchettini, J. C. (2000) *Nat. Struct. Biol. 7*, 312−321.
31. Monaco, H. L., Rizzi, M., and Coda, A. (1995) *Science 268*, 1039−1041.
32. Naylor, H. M., and Newcomer, M. E. (1999) *Biochemistry 38*, 2647−2653.
33. Semisotnov, G. V., Rodionova, N. A., Razgulyaev, O. I., Uversky, V. N., Gripas, A. F., and Gilmanshin, R. I. (1991) *Biopolymers 31*, 119−128.
34. Sebastiao, P. M., Saraiva, J. M., and Damas, M. A. (1998) *J. Biol. Chem. 38*, 24715−24722.
35. Lai, Z., Colon, W., and Kelly, J. W. (1996) *Biochemistry 35*, 6470−6482.
36. McCutchen, S. L., Colon, W., and Kelly, J. W. (1993) *Biochemistry 32*, 12119−12127.
37. Fink, A. L. (1995) *Annu. Rev. Biophys. Biomol. Struct. 24*, 495−522.
38. Ptitsyn, O. B. (1995) *Adv. Protein Chem. 47*, 83−229.
39. Serio, T. R., Cashikar, A. G., Kowal, A. S., Sawick, G. J., Moslehi, J. J., Serpell, L., Arnsdorf, M. F., and Lindquist, S. L. (2000) *Science 289*, 1317−1321.
40. Schneider, F., Hammarstrom, P., and Kelly, J. W. (2001) *Protein Sci. 10*, 1606−1613.
41. Quintas, A., Saraiva, M. J. M., and Brito, R. M. M. (1999) *J. Biol. Chem. 274*, 32943−32949.
42. Quintas, A., Vaz, D. C., Cardoso, I., and Saraiva, M. J. M. (2001) *J. Biol. Chem. 276*, 27207−27213.
43. Kraulis, P. (1991) *J. Appl. Crystallogr. 24*, 946−950.
44. Philo, J. S. (2000) *Anal. Biochem. 279*, 151−163.
45. Hammarström, P., Jiang, X., Deechongkit, S., and Kelly, J. W. (2001) *Biochemistry 40*, 11453−11459.

BI011194D